ELSEVIER

Journal of Molecular Catalysis A: Chemical 195 (2003) 173–180

JOURNAL OF MOLECULAR CATALYSIS A: CHEMICAL

www.elsevier.com/locate/molcata

Ab initio density functional study of the structural and electronic properties of an MoS_2 catalyst model: a real size $Mo_{27}S_{54}$ cluster

Hideo Orita*, Kunio Uchida, Naotsugu Itoh

National Institute of Advanced Industrial Science and Technology (AIST), Institute for Materials and Chemical Process, Tsukuba Central 5, 1-1-1 Higashi, Tsukuba, Ibaraki 305-8565, Japan

Received 8 March 2002; received in revised form 4 September 2002; accepted 17 September 2002

Abstract

Ab initio investigation of the structural and electronic properties of a real size $Mo_{27}S_{54}$ cluster has been performed to develop a fundamental understanding of the active sites of MoS_2 catalysts in the hydrotreatment process. The cluster is a stoichiometric and regular hexagonal one with $(\bar{1}\,0\,1\,0)$ plane (S edge) and $(3\,0\,\bar{3}\,0)$ plane (Mo edge) only, and does not need any saturating H atom and charge compensation. By using density functional theory (DFT) method, a full geometry optimization of the cluster has been carried out. The structure of the cluster is more relaxed towards the edges, and two types of the Mo–Mo distances, which are shorter or longer than that in the MoS_2 crystal, are observed at the periphery. These results agree well with the EXAFS data of dispersed unsupported MoS_2 particle. The electronic properties of the atoms at various sites (i.e. corner, edge, outer, and inner positions) have been distinguished clearly by means of charge distribution and molecular orbital (MO) calculations. The corner Mo atom is expected to be the most active site for the hydrotreatment reactions.

Keywords: Density functional theory; MoS_2 catalyst model; Real size cluster; Optimized structure; Electronic property

1. Introduction

Molybdenum sulfide compounds are the important active element in catalysts used in the hydrotreatment process (i.e. hydrodesulfurization (HDS) and hydrogenation (HYD)) to remove sulfur from petroleum fractions. The increasing demand to reduce the sulfur content of oil products to <50 ppm leads to a need for more efficient processes and more active catalysts. Consequently, a large number of experimental studies have been carried out to find the active sites on the catalyst surface and to examine the reaction mechanism involved in hydrotreatment (see reviews, e.g. [1,2]). It has now been known that properly reduced edges of molybdenum sulfide play the essential role in the reaction. However, the mechanism of formation of the active sites and the exact structural configuration of the atoms constituting these sites still remain unclear. Computational modeling techniques can provide one possible approach to get a better insight into the nature of active sites of the catalysts [3,4].

The crystal of MoS_2 shows a typical layered structure consisting of close-packed triangular double layers of S with each Mo atom coordinated by six S atoms in a trigonal-prismatic unit [5]. The bonding within the layers is covalent. There is only a week van der

* Corresponding author. Tel.: +81-298-61-4835; fax: +81-298-61-4634.
E-mail address: hideo-orita@aist.go.jp (H. Orita).

1381-1169/02/$ – see front matter
PII: S1381-1169(02)00528-9

Waals interaction between consecutive S–Mo–S layers. Cleaving MoS_2 between the layers results in a chemically inert (0 0 0 1) surface. It is experimentally demonstrated that for the highly dispersed supported MoS_2 catalysts, the active MoS_2 particles are small within 10–30 Å in size (10 Å = 1 nm) and sometimes constitute of a single sheet of the MoS_2 structure [1]. Therefore, it seems reasonable to use a single sheet MoS_2 cluster with the size corresponding to real MoS_2 catalyst particle as a computational model. In order to simulate the surface structure of a highly dispersed MoS_2 particle, we have chosen a regular hexagonal cluster of $Mo_{27}S_{54}$ as shown in Fig. 1 because this cluster has correct stoichiometry and eletroneutrality without any saturating H atom and charge compensation as well as its size (ca. 19 Å) is comparable to that of the real catalyst particle. Ma and Schobert [6] have discussed the reasonableness of using this cluster as the model for the highly dispersed MoS_2 particle in detail. Due to an atom-number limit in their calculation program (ZINDO), they could not calculate the $Mo_{27}S_{54}$ cluster actually. They have designed a smaller, but still stoichiometirc, $Mo_{16}S_{32}$ cluster to mimic the edge structure of the $Mo_{27}S_{54}$, and investigated the stable adsorption configuration of thiophene on the edge Mo atom. However, all the atoms are not relaxed in their simulation, and the electronic properties of the cluster were calculated without geometry optimization.

Li et al. [7] have carried out the structure optimization of the $Mo_{27}S_{54}$ cluster by using the GAMESS program. They have obtained some helpful information

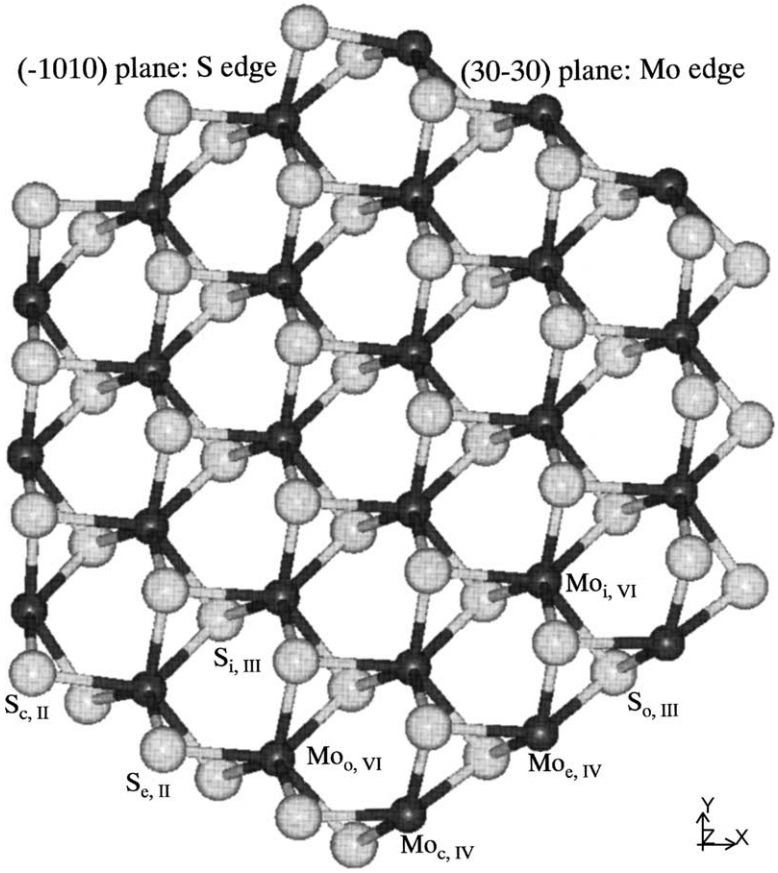

Fig. 1. Schematic representation of the $Mo_{27}S_{54}$ cluster. The dark smaller and light larger circles indicate Mo and S atoms, respectively. The cluster is rotated a little around *X*- and *Y*-axes to show the coordinative character between atoms clearly. S and Mo edge planes are indicated as (−1 0 1 0) and (3 0 −3 0) planes instead of $(\bar{1}\,0\,1\,0)$ and $(3\,0\,\bar{3}\,0)$, respectively.

on the structural and electronic properties of the cluster, and pointed out the different contributions of edge and corner sites to the frontier molecular orbitals (MO's). Their optimized geometry does not fully coincide with the EXAFS results of highly dispersed unsupported MoS_2 particle [8] because the basis they used (unrestricted Hartree-Fock (UHF)/MINI/ECP) is not a high level set. In the present work, we have performed a full geometry optimization of the $Mo_{27}S_{54}$ cluster by using density functional theory (DFT) method, and found that the computed structure agrees well with the EXAFS data. The electronic properties of various sites have been also examined.

2. Computational methods

All the calculations were performed with the program package DMol^3 (Version 4.2.1) in the Cerius^2 of Accelrys Inc. on SGI workstations of Tsukuba Advanced Computer Center (TACC) in AIST. In the DMol^3 method [9–11], the physical wave functions are expanded in terms of accurate numerical basis sets. We used the doubled numerical basis set with d-polarization functions (DND), whose size is comparable to Gaussian 6-31 G*, and effective core potential (ECP) for Mo. The generalized gradient corrected (GGA) functional, by Perdew and Wang (PW91) [12], was employed. Geometry optimization of the MoS_2 cluster started with an initial structure with coordinates of all atoms identical to those deduced from the lattice parameters of an infinite MoS_2 crystal [13], and the BFGS routine, in which the gradients were computed numerically, was employed. For the numerical integration, we used the MEDIUM quality mesh size of the program. The tolerances of energy, gradient, and displacement convergence were 2×10^{-5}, 1×10^{-2}, and 1×10^{-2}, respectively. Applying symmetry conditions to reduce the computation time was not possible when ECP was used.

3. Results and discussion

3.1. Optimized structure

The peripheral edges of the $Mo_{27}S_{54}$ cluster consist of $(\bar{1}\,0\,1\,0)$ plane (S edge) and $(3\,0\,\bar{3}\,0)$ plane (Mo edge) only. The S atoms in the cluster can be classified into four groups according to their coordinative character: the corner and edge S atoms on $(\bar{1}\,0\,1\,0)$ plane, the outer S atoms on $(3\,0\,\bar{3}\,0)$ plane, and the inner S atoms, which are symbolized by $S_{c,\,II}$, $S_{e,\,II}$, $S_{o,\,III}$, and $S_{i,\,III}$, respectively. The subscripts c, e, o, and i indicate corner, edge, outer, and inner positions of the atom, respectively. Roman numeral shows the coordinative number of each Mo atom neighboring to the S atom. According to this notation, the Mo atoms also can be classified into four groups: $Mo_{c,\,IV}$ and $Mo_{e,\,IV}$ on $(3\,0\,\bar{3}\,0)$ plane, $Mo_{o,\,VI}$ on $(\bar{1}\,0\,1\,0)$ plane, and $Mo_{i,\,VI}$. The Mo atoms on $(3\,0\,\bar{3}\,0)$ plane (i.e. $Mo_{c,\,IV}$ and $Mo_{e,\,IV}$) are 2-fold coordinatively unsaturated sites (CUS). They are usually considered as the active sites for hydrotreatment reactions, but the differences in property between the corner and edge atoms are not well understood.

The optimized structure of the $Mo_{27}S_{54}$ cluster is shown in Fig. 2 (each point corresponding to S actually represents two atoms, situated, respectively, in the upper and lower plane). The Mo–Mo distances inside the cluster (i.e. the distances between two $Mo_{i,\,VI}$'s) are between 3.16 and 3.19 Å, which corresponds well to the Mo–Mo distance in the MoS_2 crystal (3.16 Å [13]). The structure of the cluster is more relaxed towards the edges, and two types of the Mo–Mo distances are clearly observed at the periphery of the cluster. The Mo–Mo distances between the Mo atom on $(3\,0\,\bar{3}\,0)$ and $Mo_{o,\,VI}$ or $Mo_{i,\,VI}$ are shorter (ca. 3 Å) than that in the crystal, and the distances between $Mo_{o,\,VI}$ and $Mo_{i,\,VI}$ are longer (3.25–3.29 Å). Calais et al. [8] have measured EXAFS of dispersed unsupported MoS_2 particles, and observed two remarkable Mo–Mo peaks at 3.09 and 3.36 Å after subtracting the contribution of crystalline MoS_2 from the original EXAFS spectra. The EXAFS data agree well with our optimized structure of the $Mo_{27}S_{54}$ cluster. Although the edge structure under H_2/H_2S atmosphere may be different from our optimized one as simulated with infinite periodic models by Byskov et al. [14] and Raybaud et al. [15], the EXAFS spectra of MoS_2 were measured under nitrogen at room temperature after ex situ re-sulfidation at 673 K [8]. Under such a condition without H_2S, the edge of dispersed MoS_2 particle probably has a specific structure as shown in Fig. 2.

We have also performed geometry optimization of one size smaller hexagonal cluster of $Mo_{12}S_{24}$.

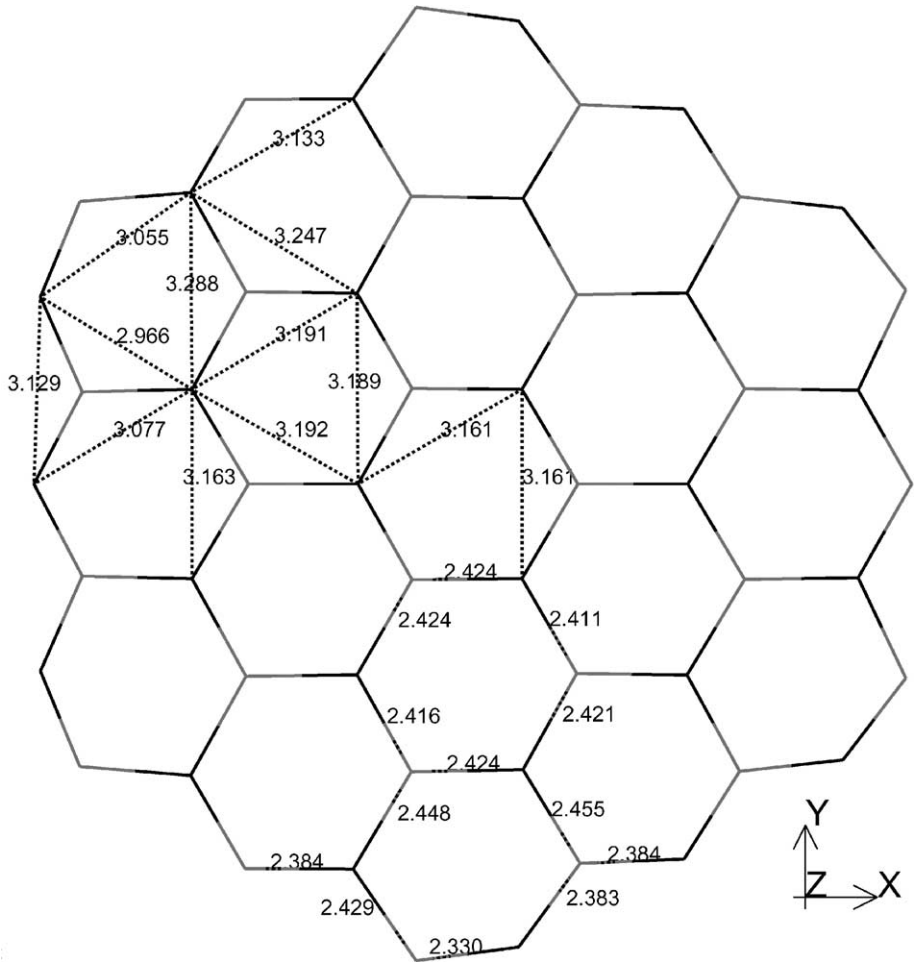

Fig. 2. Optimized structure of the $Mo_{27}S_{54}$ cluster. The characteristic distances between atoms are shown by considering the symmetry of the cluster. The dark (light) gray parts indicate Mo (S) atoms.

The peripheral structure of $Mo_{12}S_{24}$ is relaxed as that of $Mo_{27}S_{54}$, but the Mo–Mo distances inside the $Mo_{12}S_{24}$ cluster become longer to 3.27 Å. Furthermore, there is no edge atom (i.e. $Mo_{e,IV}$ and $S_{e,II}$) in this cluster. These facts indicate that the cluster size of $Mo_{12}S_{24}$ is not sufficient enough to represent the structural properties of highly dispersed MoS_2 particles although this cluster was used as a model of active phase in hydrotreatment reactions [16].

For the Mo–S distances in the $Mo_{27}S_{54}$ cluster, they are between 2.33 and 2.46 Å, which are comparable to the Mo–S distance in the MoS_2 crystal (2.42 Å). The Mo–S distances at the periphery are a little shorter. The bond between $Mo_{c,IV}$ and $S_{c,II}$ is the shortest one, which indicates that the corner site is the most relaxed in the cluster, and could be more reactive. Li et al. [7] have obtained the Mo–Mo distance of 3.50 Å and Mo–S distance of 2.52 Å for the inner part of the cluster. The deviation from the crystal structure is a little large, and their method predicts longer distances than the real values, which comes from their choice of a computationally affordable but not high level basis set.

Some Mo–Mo interactions are revealed by Mayer bond order analysis. The largest bond order of 0.56 is found between $Mo_{e,IV}$ and $Mo_{c,IV}$, indicating that there is fairly strong interaction between these

Table 1
Hirshfeld partitioned charges of the atoms in the $Mo_{27}S_{54}$ cluster

Atom group	Number	Average charge
$S_{c,\,II}$	12	−0.177 (between −0.1769 and −0.1770)
$S_{e,\,II}$	6	−0.168 (between −0.1683 and −0.1684)
$S_{o,\,III}$	12	−0.130 (between −0.1298 and −0.1302)
$S_{i,\,III}$	24	−0.107 (between −0.1041 and −0.1141)
$Mo_{c,\,IV}$	6	0.339 (between 0.3386 and 0.3396)
$Mo_{e,\,IV}$	3	0.241 (between 0.2400 and 0.2412)
$Mo_{o,\,VI}$	6	0.291 (between 0.2904 and 0.2906)
$Mo_{i,\,VI}$	12	0.228 (between 0.2259 and 0.2329)

two Mo atoms. It is worth noting that the distance (3.13 Å) is not shortest. Other characteristic bond orders between two Mo atoms are as follows; 0.49 between $Mo_{c,\,IV}$ and $Mo_{i,\,VI}$ (the shortest distance: 2.97 Å), 0.43 between $Mo_{c,\,IV}$ and $Mo_{i,\,VI}$ (the second shortest distance: 3.06 Å), 0.34 between $Mo_{e,\,IV}$ and $Mo_{i,\,VI}$ (3.08 Å), 0.26 between two $Mo_{o,\,VI}$'s (3.13 Å), 0.23–0.26 between two $Mo_{i,\,VI}$'s (3.16–3.19 Å), and 0.15 between $Mo_{o,\,VI}$ and $Mo_{i,\,VI}$ (the largest distance: 3.29 Å). As the distance between Mo atoms increases, the bond order except that between $Mo_{e,\,IV}$ and $Mo_{c,\,IV}$ tends to decrease but not linearly.

3.2. Electronic properties

The Hirshfeld partitioned charges of the atoms in the $Mo_{27}S_{54}$ cluster are tabulated in Table 1. Mulliken charges were not used in the present work because they are very dependent on the basis sets used. The Hirshfeld partitioned charges are defined relative to the deformation density. The deformation density is the difference between the molecular and the unrelaxed atomic charge densities. The Hirshfeld procedure usually produces atomic charges rather small magnitudes, but Hirshfeld charges are not so dependent on the basis sets as Mulliken. The outside layers of S are negatively charged, and the positively charged Mo plane is in the middle of the sandwiched structure. There is no overlap region of charge distribution among the atom groups, indicating that the atom groups can be distinguished clearly by charge. The charge distributions of the atoms inside the cluster ($S_{i,\,III}$ and $Mo_{i,\,VI}$) are a little broad, because each of them can be classified into further three types by considering the symmetry of the cluster strictly. The corner S atom ($S_{c,\,II}$) has the most negative charge, and the corner Mo atom ($Mo_{c,\,IV}$) possesses the most positive charge, suggesting that the atoms on the corners of a real MoS_2 catalyst show exceptionally reactive features. It is worth mentioning that the charge of $Mo_{e,\,IV}$ is smaller than that of $Mo_{o,\,VI}$ and rather comparable to that of $Mo_{i,\,VI}$. There is clear difference in charge between $Mo_{c,\,IV}$ and $Mo_{e,\,IV}$.

Table 2
Molecular orbitals of the $Mo_{27}S_{54}$ cluster located around the HOMO–LUMO region

State	Energy (eV)	Energy difference from one upper state	Occupation
HOMO − 5	−5.490	0.015	2
HOMO − 4	−5.475	0	2
HOMO − 3	−5.475	0.011	2
HOMO − 2	−5.464	0.213	2
HOMO − 1	−5.251	0	2
HOMO	−5.251	0.15	2
LUMO	−5.101	0.029	0
LUMO + 1	−5.072	0.102	0
LUMO + 2	−4.970	0	0
LUMO + 3	−4.970	0.081	0
LUMO + 4	−4.889	0	0
LUMO + 5	−4.889	0.105	0

Molecular orbital calculations and partial density of states analysis of the cluster have been also performed. Molecular orbitals located around the HOMO–LUMO region are listed in Table 2. Typical isosurfaces of MO's are represented in Figs. 3 and 4. Fig. 3 shows the isosurfaces of combination of HOMO (highest occupied molecular orbital) and HOMO − 1 because these two MO's are degenerated at the energy value of −5.251 eV. Although the MO's are distributed widely on the Mo atoms around the periphery of the cluster, they are located strongly on some of the corner Mo atoms ($Mo_{c,\,IV}$). The isosurfaces of LUMO (lowest unoccupied molecular orbital) are shown in Fig. 4. The LUMO is located dominantly on the $(3\,0\,\bar{3}\,0)$ plane and especially on the $Mo_{e,\,IV}$ atoms. Although no degenerated MO is found for LUMO, the gap between LUMO and LUMO + 1 is only 0.029 eV. The LUMO + 1 is populated strongly on the $Mo_{c,\,IV}$ atoms but not on the $Mo_{e,\,IV}$ atoms. Because of small energy differences between MO's (see Table 2), the reactivity of the cluster comes from all the MO's around the HOMO–LUMO region.

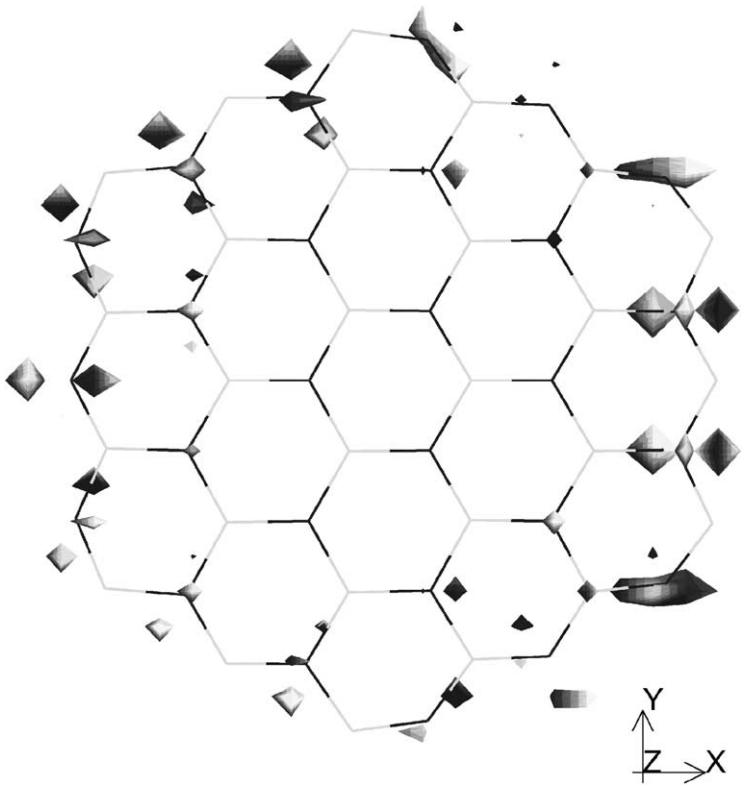

Fig. 3. Isosurfaces of combination of HOMO and HOMO − 1 of the $Mo_{27}S_{54}$ cluster.

The partial density states analysis shows that the MO's near Fermi level (HOMO − 1, HOMO, LUMO and LUMO + 1) are contributed dominantly by Mo 4d atomic orbitals and weakly by Mo 5sp, and that the contribution of S atoms is very small, which is consistent with the recent DFT calculation of Clermette et al. [17]. The computed energy difference between HOMO and LUMO is only 0.15 eV, while the MoS_2 crystal is found by using periodic calculational ability of DMol^3 [11] to be semiconducting with a gap of 0.93 eV. The calculated band gap is a little smaller than an experimental value of 1.3 eV, which can be explained by the well-known deficiency of DFT to describe occupied and unoccupied electron levels by the same functional as described in [5,18]. (The HOMO–LUMO gap calculated by Li et al. [7] is 5.86 eV, which is much larger than the band gap in the MoS_2 crystal.) The top of the valence band and the bottom of the conduction band are located at −5.12 and −4.19 eV, respectively. As the position of the top of the valence band is comparable to that of the HOMO of the cluster (−5.251 eV), it is considered that the unoccupied MO's mainly move down into the bulk-gap by the formation of CUS at the periphery of the cluster. These CUS should show the stronger acceptor properties, leading to reactions with a potential electron donor such as thiophene in the hydrotreatment process. Raybaud et al. [19] have investigated the structural and electronic properties of the $MoS_2(1\,0\,\bar{1}\,0)$ edge-surface, and showed the similar shift of states into the bulk-gap. They have concluded that the $MoS_2(1\,0\,\bar{1}\,0)$ surface is metallic in contrast to the semicondcuting bulk, and that on the unsaturated Mo-surface atoms, the most intense surface states are empty d-type states just above the Fermi level. Their results of the edge-surface agree well with ours of the cluster, showing that the used cluster is a good model to represent the electronic structure of the MoS_2 edge-surface. There is no corner site in their periodic edge-surface model although we have found the

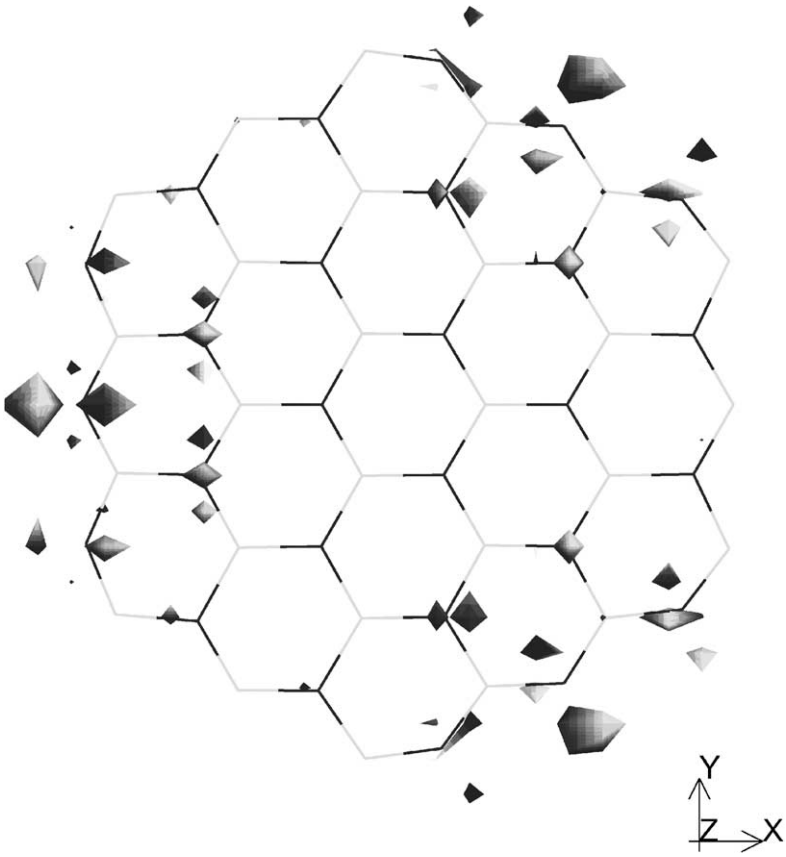

Fig. 4. Isosurfaces of LUMO of the $Mo_{27}S_{54}$ cluster.

differences in property between the corner and edge atoms. We are now extending this cluster model calculation to investigate the adsorption of thiophene on the CUS as a model for activation of sulfur-containing compounds on MoS_2 catalyst, which will be reported later elsewhere.

4. Conclusions

A full geometry optimization of a real size $Mo_{27}S_{54}$ cluster has been performed with the DFT program package DMol[3] to develop a fundamental understanding of the active sites of MoS_2 catalysts in the hydrotreatment process. The cluster is a stoichiometric and regular hexagonal one with $(\bar{1}\,0\,1\,0)$ plane (S edge) and $(3\,0\,\bar{3}\,0)$ plane (Mo edge) only, and does not need any saturating H atom and charge compensation. The atoms in the cluster can be classified into four groups according to their coordinative character: the corner, edge, outer, and inner atoms. The structure of the cluster is more relaxed towards the edges, and two types of the Mo–Mo distances are observed at the periphery. The distances between the Mo atom on $(3\,0\,\bar{3}\,0)$ plane and the outer or inner Mo atom are shorter (ca. 3 Å) than that in the MoS_2 crystal (3.16 Å), and the distances between the outer and inner atoms are longer (3.25–3.29 Å). These results agree well with the EXAFS data of dispersed unsupported MoS_2 particle.

The electronic properties of the atoms at various sites have been distinguished clearly by means of charge distribution and molecular orbital calculations. The corner S atom has the most negative charge, and the corner Mo atom possesses the most positive charge, suggesting that the atoms on the corners of a real MoS_2 catalyst show exceptionally reactive

features. The HOMO–LUMO gap of the cluster is only 0.15 eV, while the band gap of the MoS_2 crystal is computed to be 0.93 eV. It is considered that the unoccupied MO's mainly move down into the bulk-gap by the formation of CUS. These CUS should show the stronger acceptor properties, leading to reaction with a electron donor such as thiophene in the hydrotreatment process.

References

[1] A.N. Startsev, Catal. Rev. Sci. Eng. 37 (1995) 353.
[2] S. Eijsbouts, Appl. Catal. A 158 (1997) 53.
[3] R.A. van Santen, M. Neurock, Catal. Rev. Sci. Eng. 37 (1995) 557.
[4] J.W. Andzelm, A.E. Alvarado-Swaisgood, F.U. Axe, M.W. Doyle, G. Fitzgerald, C.M. Freeman, A.M. Gorman, J.-R. Hill, C.M. Kölmel, S.M. Levine, P.W. Saxe, K. Stark, L. Subramanian, M.A. van Daelen, E. Wimmer, J.M. Newsam, Catal. Today 50 (1999) 451.
[5] P. Raybaud, G. Kresse, J. Hafner, H. Toulhoat, J. Phys. Condens. Matter 9 (1997) 11085 and 11107.
[6] X. Ma, H.H. Schobert, J. Mol. Catal. A 160 (2000) 409.
[7] Y.-W. Li, X.-Y. Pang, B. Delmon, J. Phys. Chem. A 104 (2000) 11375.
[8] C. Calais, N. Matsubayashi, C. Geantet, Y. Yoshimura, H. Shimada, A. Nishijima, M. Lacroix, M. Breysse, J. Catal. 174 (1998) 130.
[9] B. Delley, J. Chem. Phys. 92 (1990) 508.
[10] B. Delley, J. Phys. Chem. 100 (1996) 6107.
[11] B. Delley, J. Chem. Phys. 113 (2000) 7756.
[12] J.P. Perdew, Y. Wang, Phys. Rev. B 45 (1992) 13244.
[13] K.D. Bronsema, J.L. de Boer, F. Jellinek, Z. Anorg. Allg. Chem. 540–541 (1986) 15.
[14] L.S. Byskov, J.K. Nørskov, B.S. Clausen, H. Topsøe, J. Catal. 187 (1999) 109;
L.S. Byskov, J.K. Nørskov, B.S. Clausen, H. Topsøe, Catal. Lett. 64 (2000) 95.
[15] P. Raybaud, J. Hafner, G. Kresse, S. Kasztelan, H. Toulhoat, J. Catal. 189 (2000) 129;
P. Raybaud, J. Hafner, G. Kresse, S. Kasztelan, H. Toulhoat, J. Catal. 190 (2000) 128.
[16] P. Faye, E. Payen, D. Bougeard, J. Catal. 179 (1998) 560;
P. Faye, E. Payen, D. Bougeard, J. Catal. 183 (1999) 396.
[17] H. Clermette, F. Rogemond, O. El Beqqali, J.F. Paul, C. Donnet, J.M. Martin, T. Le Mogne, Surf. Sci. 472 (2001) 97.
[18] R. Tokarz-Sobieraj, K. Hermann, M. Witko, A. Blume, G. Mestl, R. Schlögl, Surf. Sci. 489 (2001) 107.
[19] P. Raybaud, J. Hafner, G. Kresse, H. Toulhoat, Surf. Sci. 407 (1998) 237.